Integrated seismic image segmentation and efficient model evaluation: field data example

Adam Halpert

ABSTRACT

Salt interpretation and model building in areas with complicated salt geology represent significant bottlenecks during large iterative imaging projects. Automated tools like image segmentation can help interpreters quickly identify salt bodies in 3D seismic volumes, reducing the need for time-consuming manual picking. In addition, a scheme to efficiently test multiple possible models without fully re-migrating the dataset is useful when more than one salt scenario is in play. Here, a 3D field data example demonstrates that a combination of these two computational interpretation tools can effectively generate and test alternative models. Re-migration with a preferred velocity model produces an improved subsalt image.

INTRODUCTION

Recent increases in computing power have shifted model-building bottlenecks from computational tasks toward interpretation and similar human-intensive tasks. One approach to alleviate these bottlenecks is to develop computational interpretation tools, which can allow interpreters to take advantage of increased computational capabilities, while still allowing them to use their expertise to control the interpretation workflow. Two such tools are seismic image segmentation, and an efficient velocity model-evaluation method using synthesized wavefields. Here, I will use a 3D field data example from the Gulf of Mexico to demonstrate how these two tools can work together to effectively generate and test velocity models based on different salt scenarios, leading to an improved subsalt image.

Salt interpretation is crucial for successful model building. Because of the high velocity contrast between salt and sediments, mis-placed or mis-interpreted salt bodies can have a disproportionately negative impact on the quality of subsalt images. Seismic image segmentation is one tool interpreters can use to partially automate salt body delineation. Several individual algorithms have shown promise for this task, including the Normalized Cuts Image Segmentation scheme (Shi and Malik, 2000), which can be effectively adapted for use on 3D seismic images (Lomask, 2007; Lomask et al., 2007). In this report, I use the segmentation scheme of Felzenszwalb and Huttenlocher (2004), which can also be successfully applied to 3D seismic data (Halpert, 2010). Importantly, this method can also incorporate interpreter input and rely on

the interpreter's discretion to identify the extent of salt bodies (Halpert, 2013). These capabilities allow us to quickly generate a range of possible velocity models based on different, but plausible, salt interpretations. A way to efficiently test these models is necessary in order to avoid costly and time-consuming re-migration of very large modern 3D datasets.

Quickly updating images based on discrete changes to the velocity model is another problem with several proposed solutions. Many proposals rely on a fast, target-oriented variant of beam migration (Hill, 1990); for example, Wang et al. (2008) update post-stack images to qualitatively judge the effects of using different velocity models. An alternative is to use a similar approach but with wave-equation methods like reverse-time migration (RTM) (Wang et al., 2011); however, this remains an extremely expensive option. A different approach, first proposed by Halpert and Tang (2011), also employs wave equation imaging. However, by using an initial image and Born modeling (Stolt and Benson, 1986) to synthesize a new, targeted dataset (Tang and Biondi, 2010; Tang, 2011), the computational challenge is drastically reduced. Furthermore, if a pre-stack image with subsurface offset information is available, this method can make use of that information to identify and help correct errors in an initial velocity model.

In the following sections, I will briefly review the methods used for both the image segmentation and model evaluation parts of the computational interpretation workflow. I will then demonstrate how these tools can be applied to a 3D example from a Gulf of Mexico survey provided courtesy of WesternGeco (Figure 1(a)). Using image segmentation, I will generate a new velocity model based on a salt interpretation slightly different than the one used to create the model provided with the data (Figure 1(b)). In Figure 1, note that an inclusion within the salt body has not been assigned a velocity distinct from the rest of the salt, and that the interpretation of the base of salt is somewhat ambiguous. Both of these factors could contribute to a fading of the subsalt reflectors seen in Figure 1(a). Finally, I will compare these two models using the synthesized wavefield methodology mentioned above, and validate the comparison by showing a full re-migration of the data using the alternate model.

IMAGE SEGMENTATION

The Pairwise Region Comparison (PRC) image segmentation algorithm is a graph-cut technique based on the method of Felzenszwalb and Huttenlocher (2004). Unlike other graph partitioning algorithms such as the Normalized Cuts method (Shi and Malik, 2000; Lomask et al., 2007), it operates extremely efficiently, requiring on the order of $n \log n$ operations for an image with n pixels (compared to n^2 operations for Normalized Cuts). When adapted for use with seismic images (Halpert, 2010), this method can help identify salt bodies or other regions by constructing *edges* between each pixel in the image and several surrounding pixels. Each edge is weighted according to the largest amplitude value that exists between the two end pixels i and

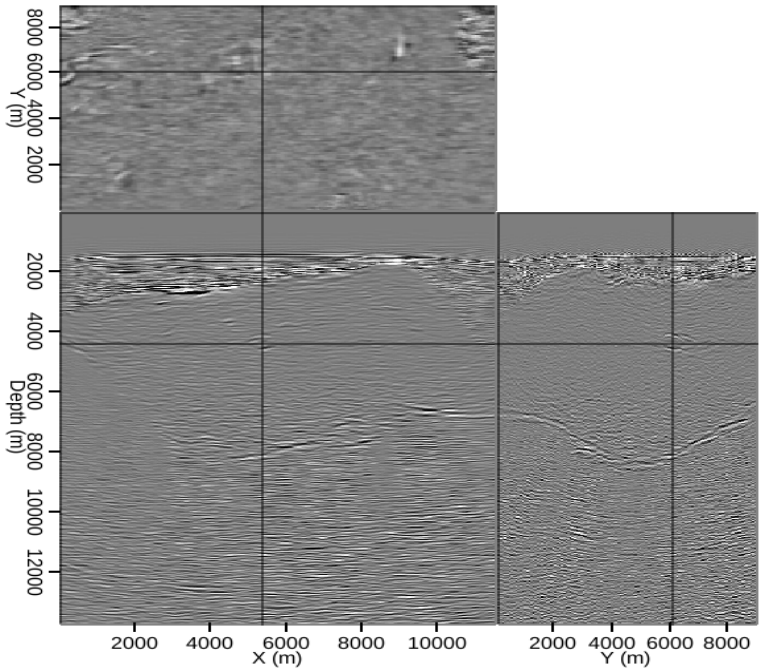

(a)

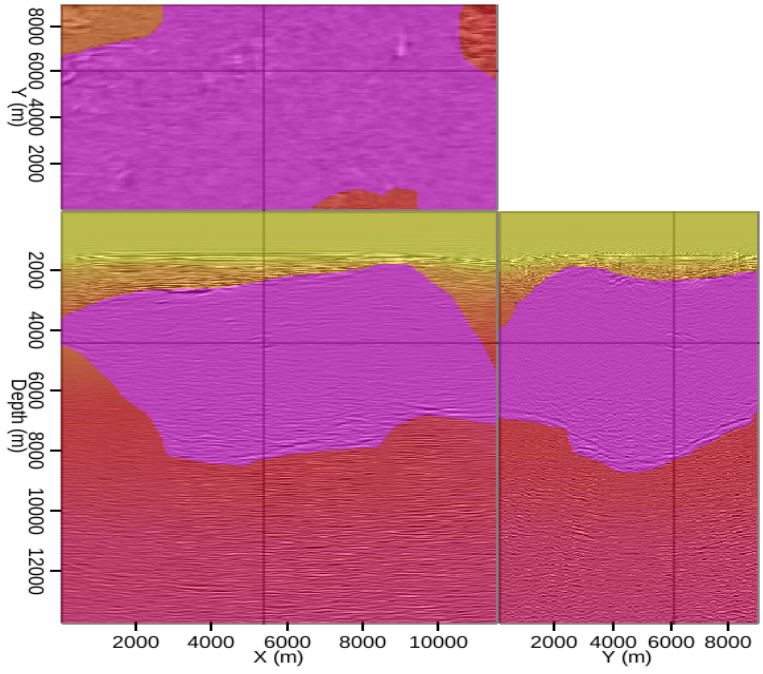

(b)

Figure 1: (a) A 3D image from the Gulf of Mexico (data courtesy of WesternGeco) obtained via one-way migration with the velocity model shown in (b). A prominent sediment inclusion within the salt body, and/or a misinterpreted base of salt, may contribute to the subsalt reflectors' loss of continuity. [**CR**]

j:

$$w_{ij} = \exp((\max I(\mathbf{p}_{ij}))^2) \exp(d_{ij}), \tag{1}$$

where $\mathbf{p}_{ij}$ is the vector of all pixels between i and j and d_{ij} is simply the Euclidean distance (in samples) between the two pixels. This approach has the effect of identifying high-amplitude edges, often indicative of salt boundaries.

Once each of the edges is assigned a weight, the segmentation of the image can proceed as described in Felzenszwalb and Huttenlocher (2004). In summary, the process begins with each pixel as its own image segment; then individual pixels, and eventually, groups of pixels, are merged according to thresholding criteria. Segments can also be merged in post-processing if they are smaller than a "minimum segment size" parameter specified by the user. Furthermore, interpreter input may be included if a fully automatic segmentation is not feasible. For a 3D segmentation, an interpreter can provide a limited manual interpretation on one or more 2D slices; this information is then "sprayed" into the third dimension to alter the input data prior to segmentation. In addition, interpreters maintain control of the process by choosing which segments to include within a salt body, for example. These chosen segments can be easily merged together, and used to create or modify an existing velocity model.

Figure 2(a) is a close-up image of the salt inclusion mentioned in the introduction. By isolating this smaller region for segmentation analysis, we are free to set the minimum segment size to a small number, allowing the automatic segmentation process to capture a higher degree of detail. Figure 2(b) is the interpreter-guided segmentation result for the salt inclusion. After following a similar process to define a new base-salt boundary, a new velocity model is produced by assigning appropriate velocities to the segmented regions. Figures 3(a) and 3(b) show the original and modified velocity models, respectively, for this region. In this case, replacement velocities were taken at appropriate depths from the background sediment velocities in areas without salt.

MODEL EVALUATION

The efficient velocity model evaluation scheme used here is based on the concept of synthesized Born-modeled wavefields (Stolt and Benson, 1986; Tang and Biondi, 2010; Tang, 2011), and was first introduced by Halpert and Tang (2011). The method also uses the "prestack exploding reflector" concept (Guerra, 2010) to identify and correct errors in an initial velocity model and its associated prestack image. The model evaluation procedure consists of three major steps (for mathematical details, see Halpert and Tang (2011)):

1. Starting from an initial image, use a form of exploding reflector modeling to "record" an areal source function at a preferred datum. Crosstalk artifacts are reduced by first having an interpreter select a horizon of interest from the

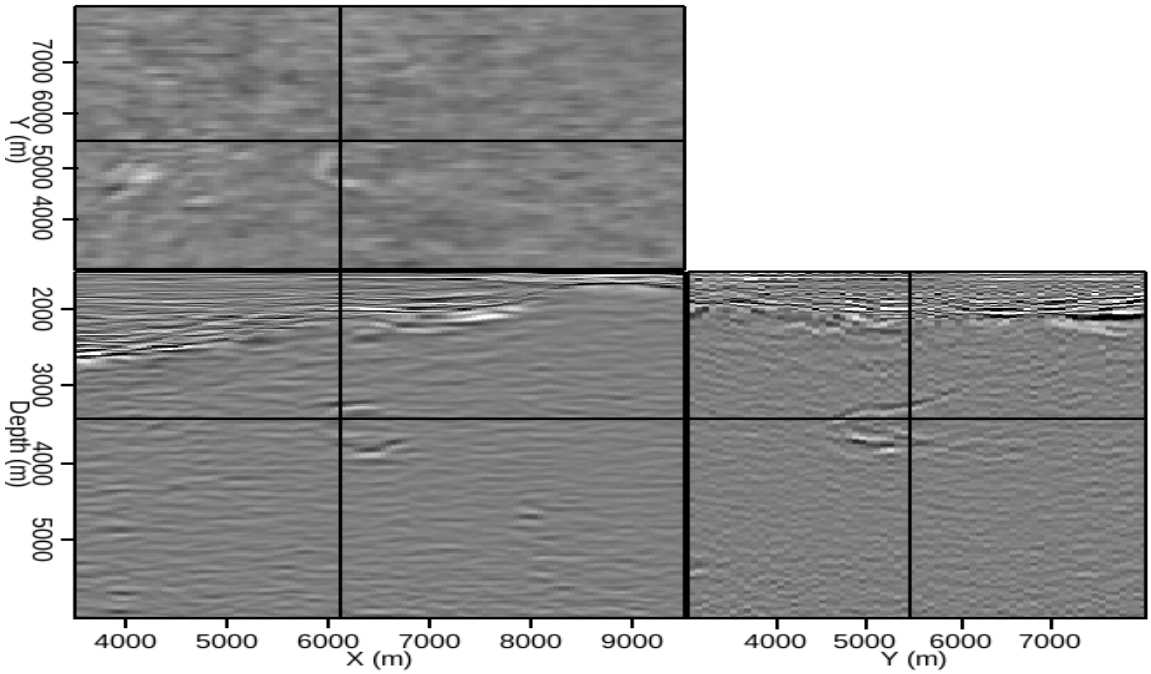

(a)

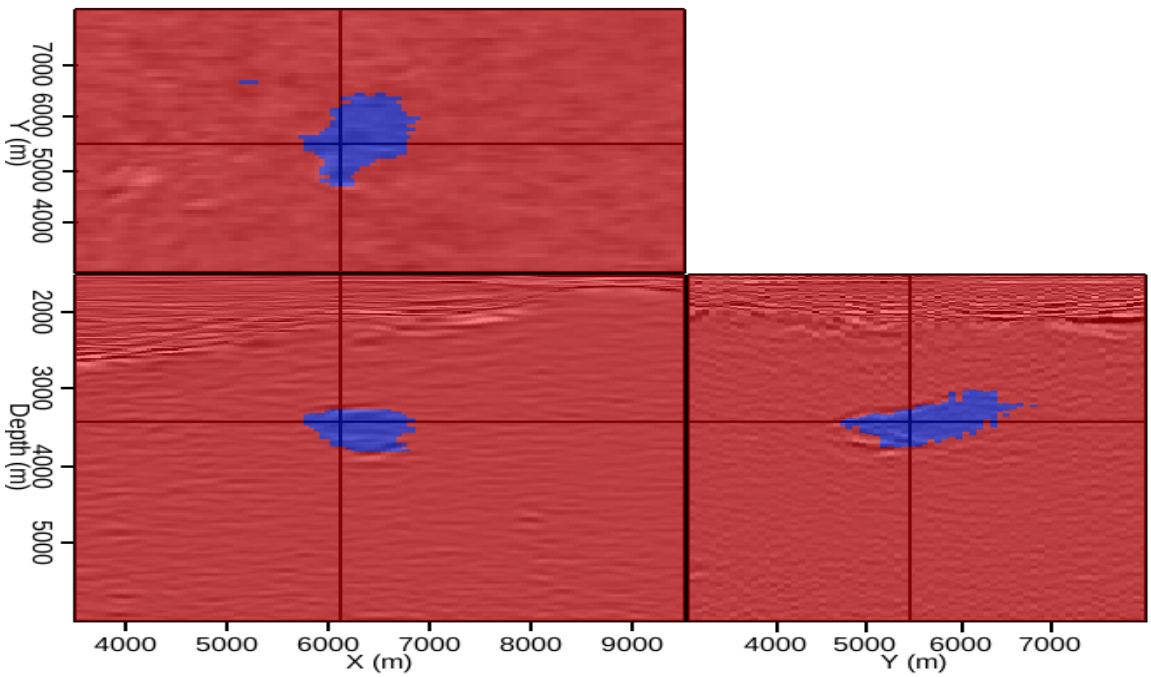

(b)

Figure 2: (a) Close-up view of the sediment inclusion first seen in Figure 1(a); (b) Interpreter-guided 3D segmentation of the image in (a). [**CR**]

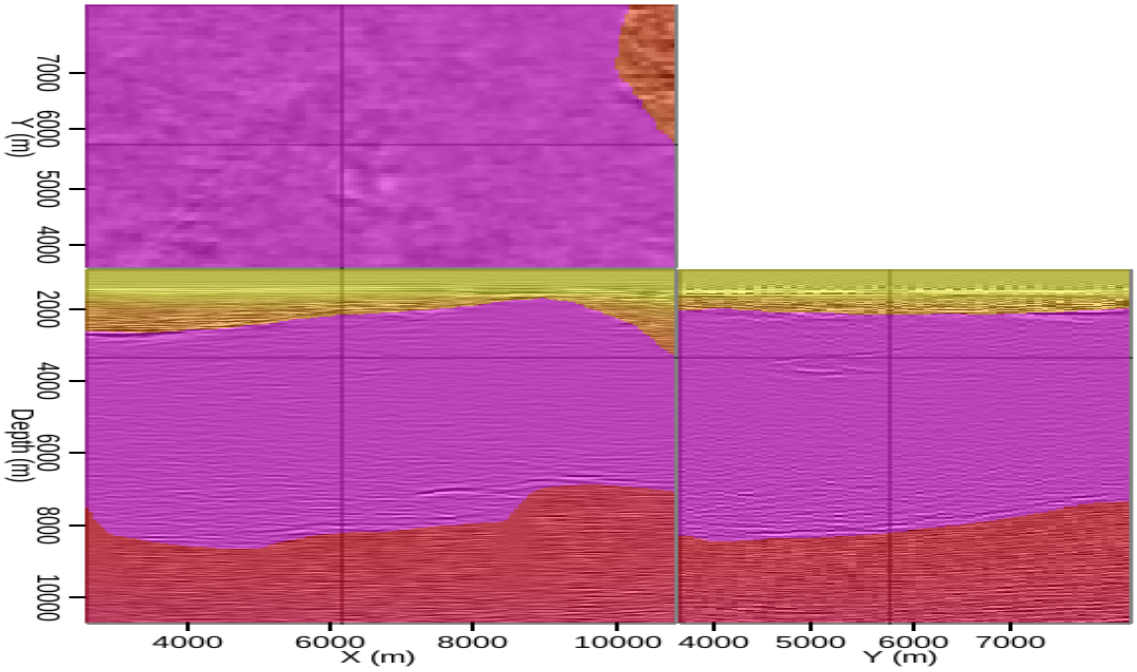

(a)

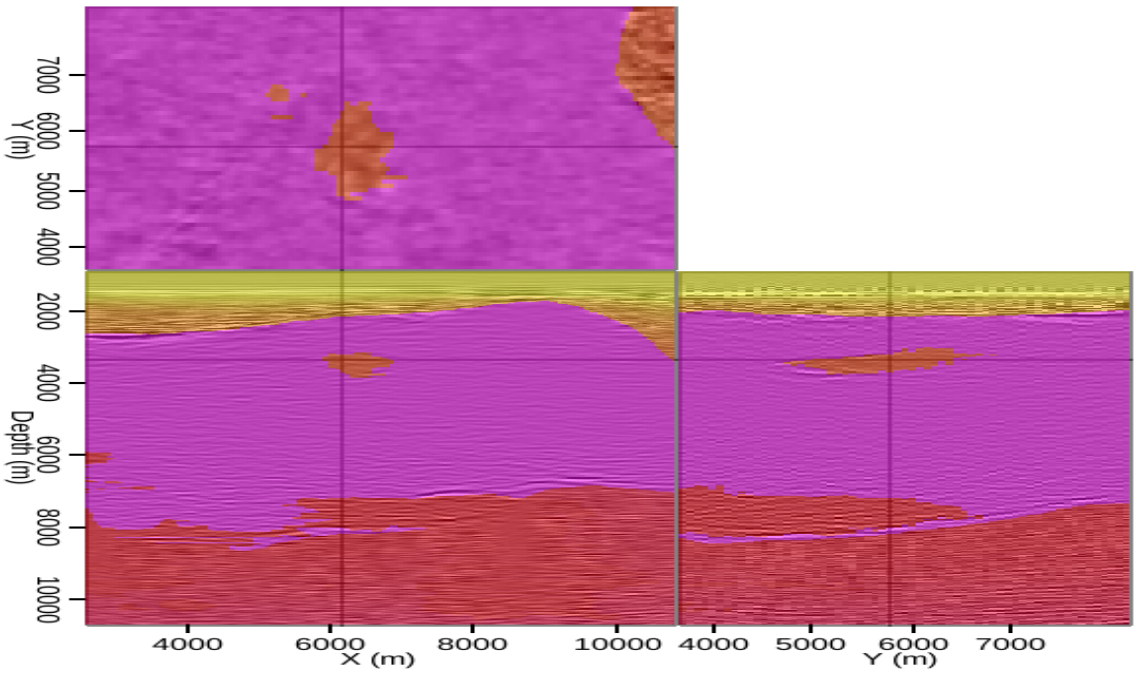

(b)

Figure 3: (a) The velocity model provided with the data; (b) An updated model based on the segmentation result in Figure 2(b) (and another defining and alternative base-salt interpretation). [**CR**]

initial image; for example, the base salt reflector indicated in Figure 4. Then, isolated points from the reflector are selected for further analysis. As long as the selected locations are separated by at least twice the maximum subsurface half-offset used from the initial image, crosstalk issues are avoided.

2. Using the new source function and the initial image as a reflectivity model, synthesize a Born-modeled dataset (Tang, 2011) with arbitrary acquisition geometry suited to the imaging target(s). As long as the same velocity model used to create the initial image is used to model this new dataset, the new receiver wavefield will be kinematically invariant of the initial model. This property is what allows us to confidently test additional models in the next step.

3. Now, the synthesized source and receiver wavefields can be imaged conventionally, using any velocity model under consideration. New images can be produced using only a single shot, a substantial computational savings over re-migrations of the full dataset.

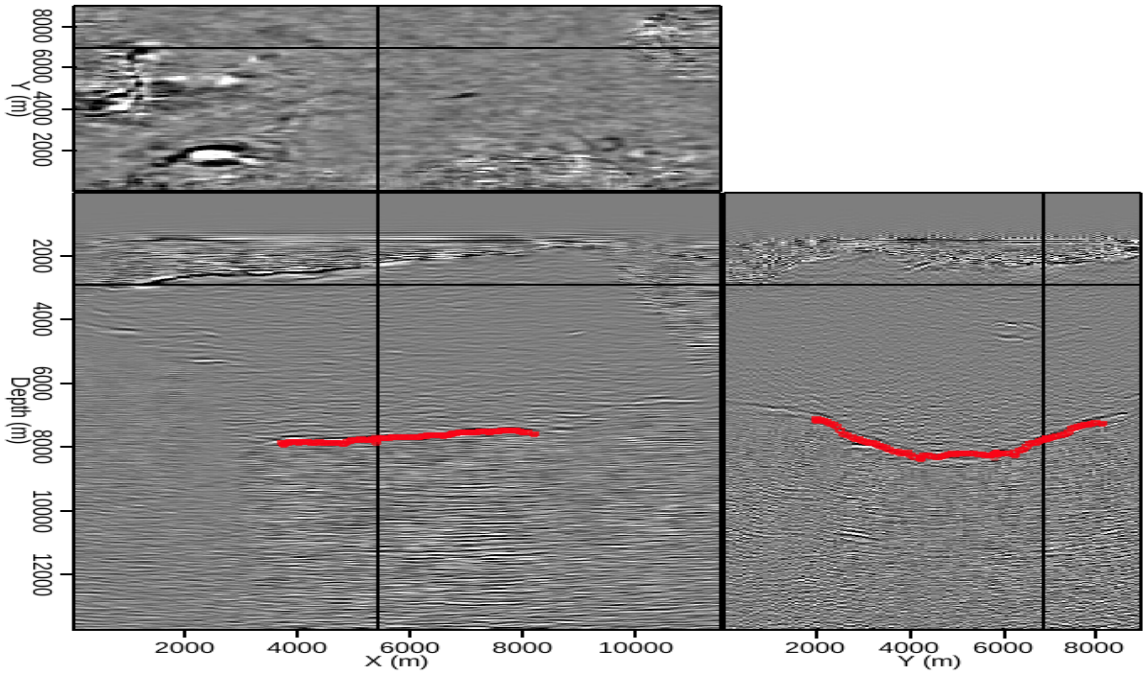

Figure 4: A manually-selected base-salt reflector that will be used to quickly evaluate the velocity models in Figure 3.

To test the models seen in Figure 3, we choose a single location from the base-salt reflector picked in Figure 4. According to the procedure outlined above, new areal source and receiver wavefields were synthesized using the initial velocity model. Then, the location isolated from the picked reflector was imaged using the two different models. The results in Figure 5 are qualitatively extremely similar, although a slight increase in focusing may be detected along the crossline direction in Figure 5(b). A

larger difference between the two images can be detected by examining the subsurface offset domain; Figures 6(a) and 6(b) show this information taken from the x, y, z location indicated in Figure 5. Now, a higher degree of focusing is more evident in the image obtained using the new model (Figure 6(b)). However, a quantitative measure of image focusing is still desirable, especially when the images are difficult to judge qualitatively, as is the case here. To measure image focusing, we use

$$F = \frac{\sum_{i=\mathbf{p}} |A_i|}{\sum_{i=\mathbf{p}} |A_i| \exp\left(\alpha \frac{|h_i|}{h_{\max}}\right)}, \tag{2}$$

where $\mathbf{p}$ is the set of all image points, A_i is the amplitude at a given point, h_i is the subsurface offset at that point, and α is an optional user-specified weighting parameter. Using this measure, a value of $F = 1$ means that all energy is perfectly focused at zero offset; as F decreases toward zero the image becomes progressively less focused. In this case, the F value for the image obtained using the original velocity model was 0.727, while the new model yielded an F value of 0.736, indicating that the new model provides a better-focused image at that location.

To test the prediction of the model evaluation procedure, full migrations were performed using both of the tested models. Figures 7(a) and 7(b) are images produced using the original and new models, respectively. Both migrations were performed using a one-way, split-step Fourier method with interpolation, using identical parameters. There are clear differences between the two results, and in our subsalt target area, the new model has produced a superior result, especially at the indicated locations.

CONCLUSIONS

Computational interpretation tools such as interpreter-guided image segmentation and efficient model evaluation using synthesized wavefields can effectively add automation to an interpreter-driven model building workflow. In this example, image segmentation was used to delineate a salt body inclusion and define a base salt slightly different from an original model. To test a new model derived from these segmentations, Born-modeled wavefields were synthesized and used to quickly (in a single shot) image an isolated location from a key reflector. Qualitative and quantitative analysis suggested that the new model would produce a better-focused image; full migrations using both models confirmed that the updated model produced improved continuity in subsalt reflectors. Creation and testing of additional models would be straightforward, and could yield even better results.

ACKNOWLEDGMENTS

I am grateful to Yaxun Tang for his contributions to the Born wavefield modeling framework, and to WesternGeco for providing the data and initial model used in the example.

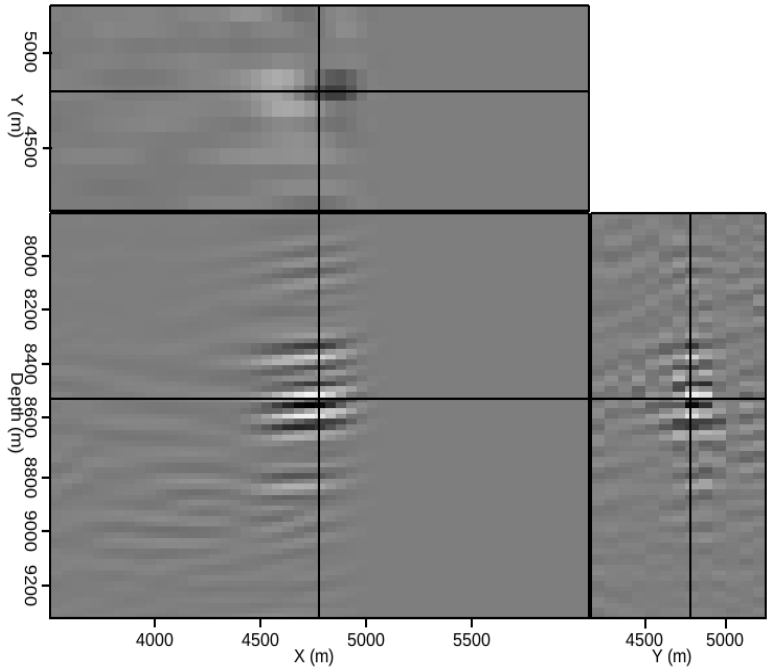

(a)

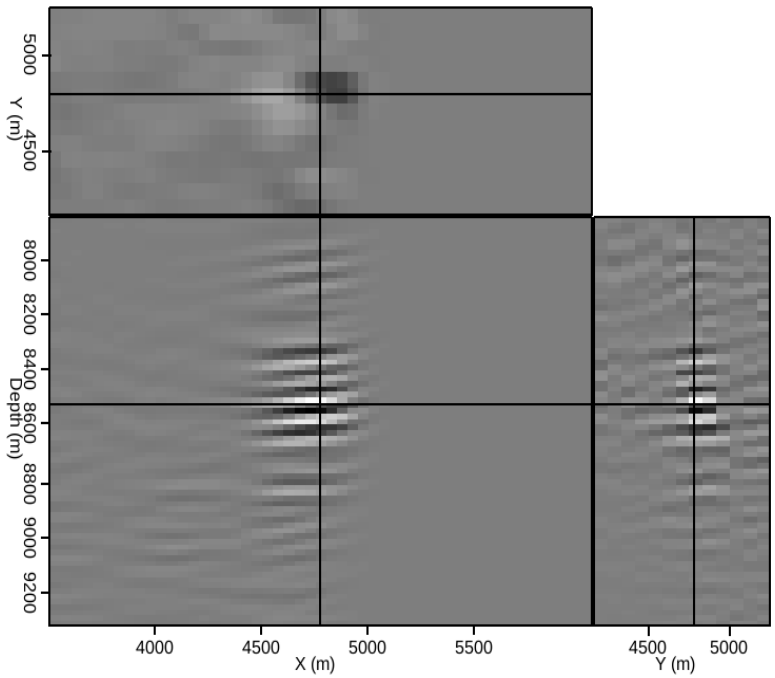

(b)

Figure 5: An isolated location from the reflector in Figure 4, quickly imaged using (a) the original velocity model; and (b) the updated model. [**CR**]

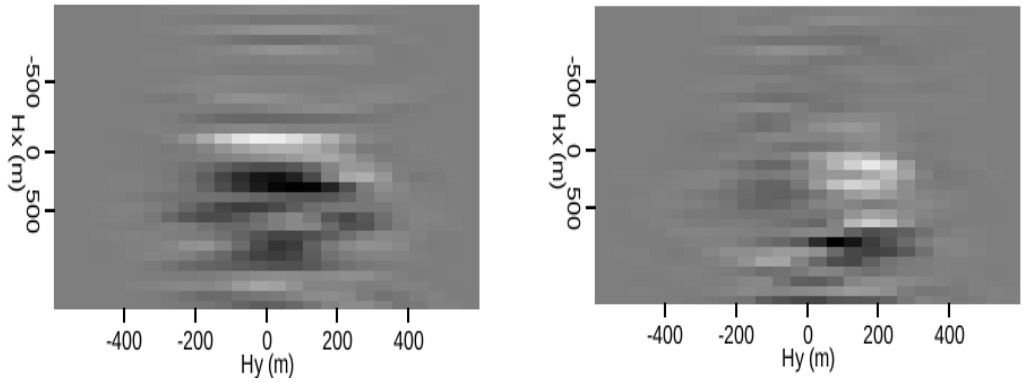

Figure 6: Subsurface offset panels at a single x, y, z location indicated in Figure 5 for the image corresponding to (a) the original velocity model; and (b) the updated model. [**CR**]

REFERENCES

Felzenszwalb, P. F. and D. P. Huttenlocher, 2004, Efficient graph-based image segmentation: International Journal of Computer Vision, **59**, 167–181.

Guerra, C., 2010, Migration-velocity analysis using image-space generalized wavefields: PhD thesis, Stanford University.

Halpert, A., 2010, A new method for more efficient seismic image segmentation: SEP-Report, **140**, 213–228.

———, 2013, Salt delineation via interpreter-guided 3D seismic image segmentation: SEP-Report, **149**, 107–120.

Halpert, A. and Y. Tang, 2011, Velocity model evaluation through Born modeling and migration: a feasibility study: SEP-Report, **145**, 15–26.

Hill, N. R., 1990, Gaussian beam migration: Geophysics, **55**, 1416–1428.

Lomask, J., 2007, Seismic volumetric flattening and segmentation: PhD thesis, Stanford University.

Lomask, J., R. G. Clapp, and B. Biondi, 2007, Application of image segmentation to tracking 3D salt boundaries: Geophysics, **72**, P47–P56.

Shi, J. and J. Malik, 2000, Normalized cuts and image segmentation: Institute of Electrical and Electronics Engineers Transactions on Pattern Analysis and Machine Intelligence, **22**, 838–905.

Stolt, R. H. and A. Benson, 1986, Seismic migration: Theory and practice: Geophysical Press.

Tang, Y., 2011, Imaging and velocity analysis by target-oriented wavefield inversion: PhD thesis, Stanford University.

Tang, Y. and B. Biondi, 2010, Target-oriented wavefield tomography using demigrated Born data: SEP-Report, **140**, 67–82.

Wang, B., J. Ji, C. Mason, S. Gajawada, and Y. Kim, 2008, Beam-based interactive imaging for salt interpretation and salt model building: SEG Technical Program

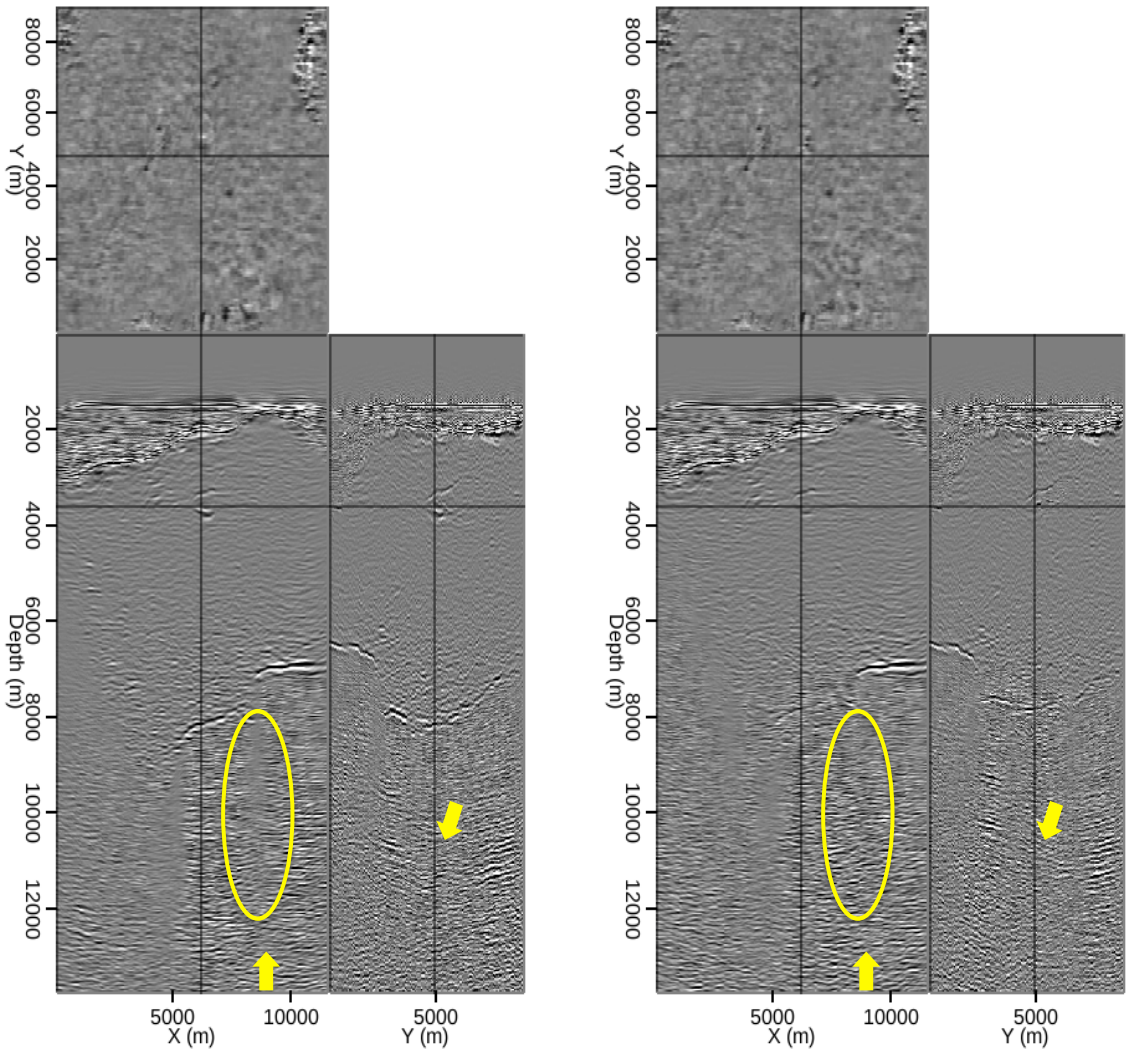

Figure 7: Full, one-way migrations with identical parameters using (a) the original velocity model; and (b) the updated model. Improvements in subsalt reflectors' continuity is apparent in (b), especially at the indicated locations. [**CR**]

Expanded Abstracts, **27**, 3073–3077.

Wang, B., C. Mason, K. Yoon, J. Ji, J. Cai, S. Suh, and Z. Li, 2011, Complex salt model building using a combination of interactive imaging and layer-stripping RTM: First Break, **29**, 47–54.